Journal of Catalysis **211,** 235–243 (2002)
doi:10.1006/jcat.2002.3705

Propane Oxidation on Mo–V–Sb–Nb Mixed Oxide Catalysts

2. Influence of Catalyst Activation Methods on the Reaction Mechanism

Ekaterina K. Novakova, Jacques C. Védrine,[1] and Eric G. Derouane

Leverhulme Centre for Innovative Catalysis, Department of Chemistry, The University of Liverpool, Oxford Street, Liverpool, L69 7ZD, United Kingdom

Received March 25, 2002; revised May 30, 2002; accepted May 30, 2002

This work aims at demonstrating a relationship between the propane oxidation reaction mechanism and the chemical/physical properties of the Mo–V–Sb–Nb mixed oxide catalyst, calcined (500/600°C) and activated (500°C) under oxidative and inert conditions. Calcination and activation under inert conditions yields a catalyst with complex mixed oxides phases ($Sb_4Mo_{10}O_{31}$, $(M_y^{5+}\,Mo_z^{5+}Mo_{1-y-z}^{6+})_5O_{14}$, etc.) and a partial reduced total oxidation state, which favours the formation of propene as the sole primary product and acrylic acid as a major secondary product. In contrast, catalysts calcined and/or activated in an oxidative atmosphere give more oxidised phases (MoO_3 as a major phase), which results in the preferable formation of acetic acid via a route which bypasses propene as an intermediate.

Key Words: **propane; propene; oxidation; reaction pathways; active phases; Mo–V–Sb–Nb oxides; XRD; ESR; XPS.**

INTRODUCTION

The direct oxidation of propane to acrylic acid using molecular oxygen as oxidant has recently attracted a lot of attention in both academia and industry, for fundamental reasons, concerning alkane activation and oxygen insertion, and for economic reasons, given the high abundance in natural gas of propane, which is lower in price than propene. A large variety of catalysts have been studied for the direct oxidation of propane to acrylic acid, but to date none has shown catalytic performance at a level required for industrial application. Three main groups of materials have been investigated, including VPO-type catalysts (1–4), which are successfully applied in industry for the oxidation of *n*-butane to maleic anhydride (5), heteropoly compounds (6–9), and mixed oxide catalysts (10–14). They have different physicochemical properties due to their different chemical natures, and the methods of preparation and heat pretreatment are very important in controlling them. This results in significant variations in catalytic performance (15).

[1] To whom correspondence should be addressed. Fax: +44 151 794 3587. E-mail: vedrine@liv.ac.uk.

The most promising catalyst appears to be the Mo–V–Te(Sb)–Nb mixed oxide system, initially proposed by Mitsubishi Chemicals as an active and selective catalyst for propane ammoxidation to acrylonitrile (16, 17) and propane oxidation to acrylic acid (18). However, it has been shown that the choice of preparation method (10, 19) and calcination conditions (20) is crucial for the formation of certain crystalline-phase structures (multiphase or single-phase materials) and subsequently for their activity and selectivity to acrylic acid.

This article aims at demonstrating the influence of different calcination and activation procedures of a catalyst with the elemental composition $Mo_1V_{0.3}Sb_{0.25}Nb_{0.08}O_n$ on the reaction network of propane oxidation. Significantly different reaction networks are proposed in the literature when propane oxidation is carried out over V–P–O catalysts (1), Te–P/NiMoO catalysts (13), Mo–V–Te–Nb–O catalysts (21, 22), and VO–H–beta zeolite catalysts (22). The differences observed can be attributed not only to the elemental composition of the catalysts, but also to their physicochemical properties, such as reducibility and acidity, as demonstrated by Luo *et al.* (22). One way to modify these properties is by varying the conditions of calcination and activation in the reactor prior to reaction. Part 1 of this study (23) deals with a kinetic and mechanistic investigation using only one catalyst calcined at 600°C in a flow of air and activated at 500°C in O_2/He. In this follow-up study, the results from part 1 will be combined with those obtained using two other catalysts calcined and activated under conditions different than the above.

EXPERIMENTAL AND METHODS

The catalysts were prepared by a coprecipitation method, described in detail in part 1 of this work (23). The catalyst precursor with the elemental composition $Mo_1V_{0.3}Sb_{0.25}Nb_{0.08}O_n$ was calcined under two different sets of conditions: (a) 600°C under a flow of predried air for 2 h and (b) 500°C under a flow of nitrogen for 2 h. The sample calcined under condition (a) was further activated

0021-9517/02 $35.00

in situ prior to reaction at 500°C in a flow of 20% O_2 in He, whereas the one calcined under condition (b) was activated at 500°C in an oxidative atmosphere (20% O_2/He) or in an inert atmosphere (pure He). The choice of conditions was based on our study of the effect of activation methods (24) and represents the extreme cases of physical properties and catalytic performance. The catalysts were characterised using BET, XRD, H_2-TPR, NH_3-TPD, ESR, and XPS techniques, as outlined in part 1 (23). ESR spectra were recorded on a Varian E109 spectrometer at X-band frequencies (9.145 GHz; 100-kHz field modulation) at room temperature and −173°C. All the parameters were calculated against a DPPH standard ($g = 2.0036$). XPS analyses were performed using a VG Scientific apparatus with a Mg anode as a source of nonmonochromatised X-ray radiation, operating at 50 eV. All binding energies were measured using the C 1s line as a standard (284.5 eV). The reaction was carried out in a continuous flow, fixed-bed microreactor, the setup of which is described in detail in part 1 of this work.

The determination of the reaction network over these three catalysts was done by performing propane and propene oxidation reactions independently as a function of the total gas hourly space velocity (i.e., the total flow rate) in the range 1500–6000 h^{-1} over 1 and 0.7 g of catalyst (particle size, <150 μm) diluted in SiC to a total catalytic bed volume of 1.2 ml for propane and propene oxidation experiments, respectively. The reactions were performed at 400°C using feed composition: 52 vol% C_3H_8(C_3H_6), 13 vol% O_2, and 35 vol% H_2O. A blank reaction (SiC only, 1.2 ml) was carried out prior to conducting the mechanistic study and did not show any activity, nor was there occurrence of homogenous combustion of propane since the sample was placed between two layers of quartz wool. The results are extrapolated to zero contact time by using linear and polynomial fitting functions.

For all experiments, the reactant conversion was calculated as the number of moles of C in all products assuming 100% carbon balance with respect to the number of moles of C introduced. The selectivity towards a product was taken as the fraction of the moles of C in the product with respect to the total moles of C in all products. The moles of C were defined as the number of moles multiplied by the number of C atoms in the reactant/product.

RESULTS AND DISCUSSION

Catalysts Characterisation

The three catalysts used have the same chemical composition but different crystalline structures and redox and acidic properties. The differences in the physical states of these materials were achieved by varying the conditions of calcination and *in situ* activation in the reactor prior to the reaction, as outlined above. The BET analyses show

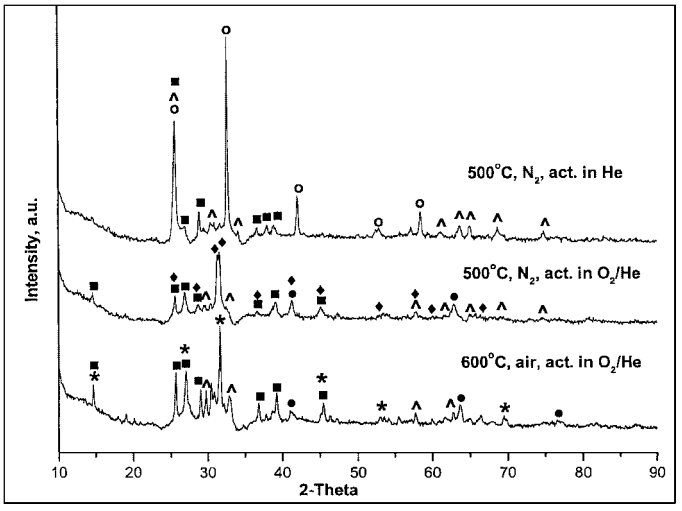

FIG. 1. XRD patterns of $Mo_1V_{0.3}Sb_{0.25}Nb_{0.08}O_n$ catalysts calcined and activated under different conditions before catalytic testing: ✱, MoO_3 (JCPDS: 35-0609); ^, Mo_8O_{23} (05-0339); ■, $(V_{0.07}Mo_{0.93})_5O_{14}$ (31-1437) and $Nb_{0.09}Mo_{0.91}O_{2.8}$ (27-1310); ●, $VSbO_4$ (35-1485); O, $Sb_4Mo_{10}O_{31}$ (33-0104); and ◆, $Sb_2Mo_{10}O_{31}$ (33-105).

that the catalyst calcined in air has a slightly higher surface area than that in nitrogen (6.9 and 6.1 $m^2\ g^{-1}$, respectively). The *in situ* activation in oxidative or inert atmosphere does not lead to a change in the surface area of the catalst. The XRD patterns of these materials are significantly different depending on the calcination and activation conditions, as illustrated on Fig. 1. For the catalyst calcined in air and activated in O_2/He (23), the major crystalline phase present is assigned to MoO_3 together with Mo_8O_{23} and $VSbO_4$ phases and a phase of type $(M_y^{5+}Mo_z^{5+}Mo_{1-y-z}^{6+})_5O_{14}$, where $M = V$ ($y = 0.09$, $z = 0.31$) and/or Nb ($y = 0.07$, $z = 0.33$). In addition, a broad band centred approximately at 2θ 30° indicates the presence of amorphous material. In the case of the catalyst calcined in nitrogen and activated in pure helium, the major phase is the $Sb_4Mo_{10}O_{31}$ phase in conjunction with the $(M_y^{5+}Mo_z^{5+}Mo_{1-y-z}^{6+})_5O_{14}$-type phases. *In situ* activation in an oxidative atmosphere (20% O_2 in He) leads to modification in the phase distribution of the nitrogen-calcined samples, as the major phase ($Sb_4Mo_{10}O_{31}$) in the case of helium activation disappears and is replaced by a more-oxidised Sb–Mo–O phase ($Sb_2Mo_{10}O_{31}$). The other phases found are Mo_8O_{23}, $VSbO_4$, and $(M_y^{5+}Mo_z^{5+}Mo_{1-y-z}^{6+})_5O_{14}$. It is clear then that activation in an oxidative atmosphere produces a catalyst with an intermediate crystalline-phase distribution compared to the other two cases. Therefore, if the catalytic behaviour is determined by the presence of these phases, a certain sequence in product selectivity with catalyst structure should be observed.

H_2-TPR experiments showed that these materials reduce to a high extent at high temperatures, but at temperatures below 600°C, only 2% of the total reducible species undergoes a reduction. However, it is worth noting that the degree

TABLE 1

Surface Composition of Catalysts Calcined in Air and Nitrogen Found by XPS and Compared to the Atomic Absorption Analysis

Element	Calcination		AA analysis
	Air	Nitrogen	
Mo $3d_{5/2}$	1	1	1
V $2p_{3/2}$	0.31	0.31	0.30
Sb $3d_{3/2}$	0.62	0.25	0.25
Nb $3d_{5/2}$	0.04	0.1	0.08

of total reducibility is significantly different for the air- and nitrogen-calcined samples, implying that calcination under nitrogen leads to partial reduction of the catalyst precursor. It is demonstrated also by the shift in the temperature at which the reduction occurs, which for the nitrogen-calcined sample is nearly 100°C higher than for air-calcined one.

The partial reduction during calcination in nitrogen is further demonstrated by the XPS and ESR measurements. XPS analyses have been performed on the catalysts calcined at 600°C in air and at 500°C in nitrogen. Quantitative data on the surface composition of metal cations are reported in Table 1. It appears that upon calcination in air, there is diffusion of cations from the bulk to the surface, resulting in higher amounts of Sb and a deficiency of Nb in comparison to that shown in the atomic absorption data. With the nitrogen-calcined catalyst, surface and bulk compositions are very similar. Considering the binding energies of the XPS peaks (Table 2), it appears that the majority of the metal cations are in their highest oxidation state. The only exceptions are Sb^{3+} (in the case of calcination in nitrogen) and some presence of V^{4+} and Mo^{5+}, suggested by the peak shape of V 2p and Mo 3d (broader peaks, shifts towards lower binding energy values) (Fig. 2).

The ESR characterisation clearly shows the presence of Mo^{5+} cations in all three catalysts in amounts estimated

TABLE 2

Binding Energies and Proposed Oxidation States of the Catalysts Calcined in Air and Nitrogen

Element	Calcination in air		Calcination in nitrogen		Handbook of XPS
	Binding energy (eV)	Oxidation state	Binding energy (eV)	Oxidation state	
Mo $3d_{5/2}$	232.2	6+, 5+	232.3	6+, 5+	MoO_2—229.2 MoO_3—232.3
V $2p_{3/2}$	516.6	5+, 4+	516.2	5+, 4+	VO_2—515.9 V_2O_5—516.8
Sb $3d_{3/2}$	540.1	5+	539.5	3+	Sb_2O_3—539.4 Sb_2O_5—540.2
Nb $3d_{5/2}$	206.6	5+	206.3	5+	NbO_2—205.9 Nb_2O_5—207.0

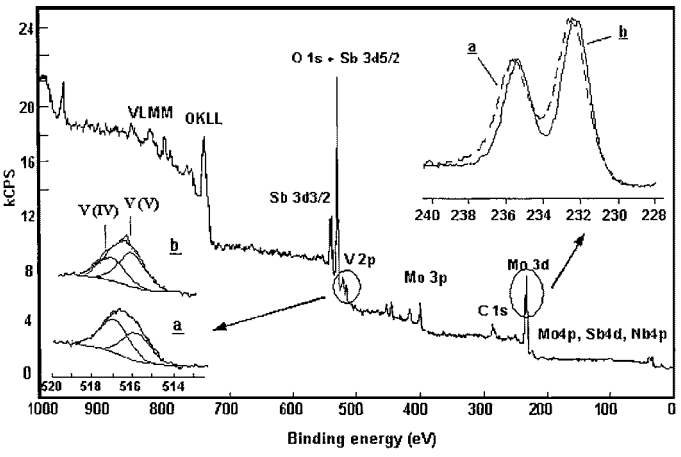

FIG. 2. XPS spectra of catalysts (a) calcined in nitrogen and (b) calcined in air (expansion of the peaks due to Mo 3d and V 2p binding energies).

at 14% for the air-calcined catalyst and at 10 and 19% for the nitrogen-calcined samples activated in O_2/He and He, respectively. The shape of the Mo peak is symmetrical, which is indicative of a strong unpaired electron exchange, i.e., Mo^{5+} is certainly embedded within a crystalline phase rather than an isolated ion at the surface (Fig. 3). Additionally, well-dispersed V^{4+} species are observed with calcination in nitrogen and determined to be in two different environments as a result of eight well-resolved lines due to the hyperfine structure ($I = 7/2$).

H_2-TPR, XPS, and ESR demonstrated that when the catalysts are calcined in nitrogen, more reduced species

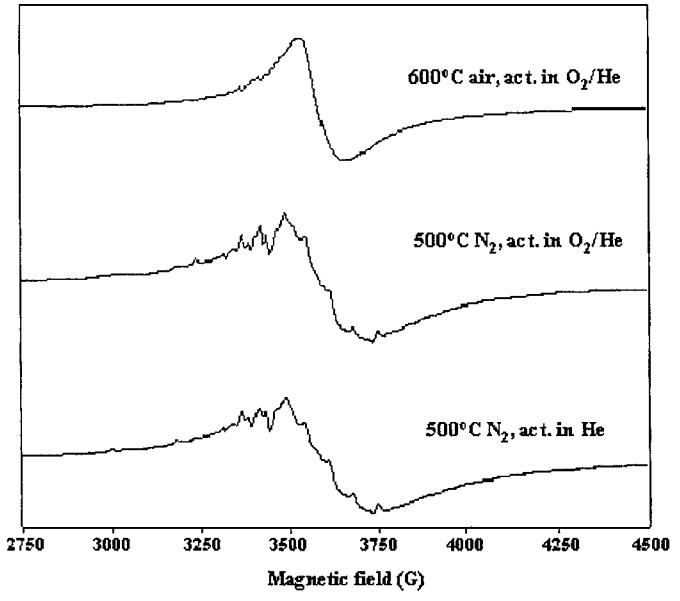

FIG. 3. ESR spectra of the $Mo_1V_{0.3}Sb_{0.25}Nb_{0.08}$ mixed oxide catalyst calcined and activated under different conditions, recorded at room temperature under vacuum, and normalised to the same gain value of 100 kHz.

are formed. Hence, less lattice oxygen is available for the hydrocarbon oxidation with catalysts calcined in nitrogen.

Another important property of the catalyst, which can determine the reaction pathways and product distribution, is the acidity of the catalysts, measured by NH_3-TPD. We found that the catalysts studied are only weakly acidic, with pK_a values, determined from calibration with NH_4-MFI zeolites (Si/Al = 18, 47, and 180), of 5.9 and 6.8 for air- and nitrogen-calcined samples, respectively, and a predominant presence of weak and medium acidic sites. The implication of this in terms of catalyst performance lies in the suppressed carbon oxide formation, which is normally enhanced by the presence of high acidity.

Propene Oxidation

The determination of the propane oxidation reaction network can be improved by studying independently propene and propane oxidation over each catalyst and plotting the selectivity of the products against contact time. The contact time varied in a range between 0.5 and 2.5 s. The microreactor used for this study did not allow contact times lower than 0.5 s because of too-high turbulence in the reactant feed flow. Primary products had nonzero intercept at zero contact time whereas secondary or higher order products appeared at a positive contact time. The reaction conditions were selected to minimise the formation of total oxidation products in the experiments at low conversion and under hydrocarbon-rich feed conditions.

Propene oxidation over the catalyst calcined in air (23) gave three products at 0-s contact time (acrolein, acetone, and acrylic acid), but only the first two were assigned to primary products, as their selectivity curves decreased with contact time (Fig. 4). Acrylic acid showed behaviour of a secondary product, which formed rapidly in the course of the reaction, and even at very low contact times, its amount was substantial. Acetic, acid, CO, and CO_2 are typical secondary products initialy formed at positive contact times. Finally, propionic acid was formed in trace quantities. Stationary formation of all products was reached at contact times higher than 1 s.

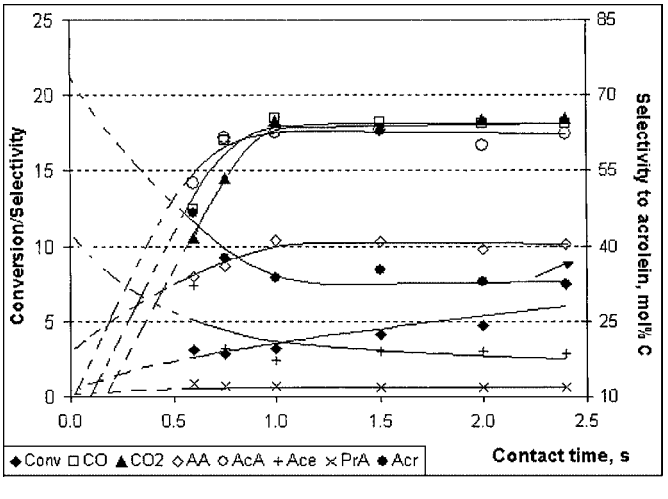

FIG. 4. Conversion/selectivity (mol% C) vs contact time for propene oxidation with catalyst calcined at 600°C in air, activated at 500°C in O_2/He (AA, acrylic acid; AcA, acetic acid; Acr, acrolein; Ace, acetone; and PrA, propionic acid).

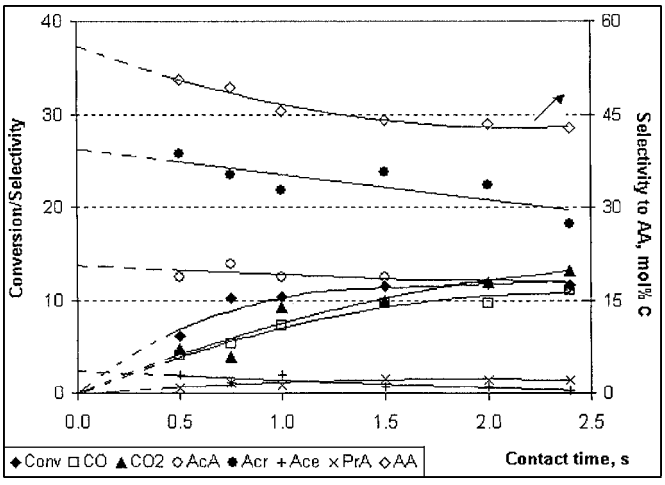

FIG. 5. Conversion/selectivity (mol% C) vs contact time for propene oxidation with catalyst calcined at 500°C in nitrogen, activated at 500°C in O_2/He (abbreviations as in Fig. 4).

When propene oxidation is performed over the catalyst calcined in nitrogen and activated in O_2/He, higher activity and selectivities towards the oxygenated products are observed compared to the sample calcined at 600°C in air. An illustration of this is the higher propene conversions. Five products are observed at zero contact time: acrylic acid, acrolein, acetic acid, CO, and acetone (Fig. 5). It is still noticeable that acrolein and acetone are primary products, as their selectivities decrease more rapidly with increase in contact time compared to acrylic and acetic acids selectivities. Acrylic acid selectivity decreases at very short contact times but becomes steady at contact times greater than 1 s. The opposite trend is observed for CO selectivity at short contact times, which is indicative of further oxidation of acrylic acid to CO. Acetic acid trend remains quite stable with contact time; very small decrease in the selectivity ($\approx$2%) is observed between the two extreme contact times studied.

The extrapolation of the CO_2 trend suggests that this product should start from a very low positive contact time. It is important to note that at contact times shorter than 1 s, there is no apparent relationship between acetic acid and CO_x formation, which are products of C–C cleavage of the C_3 molecule. A possible explanation could be the different rates of formation and/or desorption of the two products, implying a mismatch in the detection at very short contact times.

Propionic acid is again a minor product (average selectivity of 1.2 mol% C), formed at positive contact time. Its

selectivity increases steadily with contact time, which may indicate that propionic acid is a more stable product than acrylic and acetic acids and does not oxidise further.

The catalyst calcined in nitrogen and activated in helium shows the highest activity and selectivities when compared to the previous examples. Furthermore, propene conversion reaches the theoretical value of 14.2% for total conversion at contact times greater than 1 s (Fig. 6). This means that no information about the reaction network can be extracted at contact times greater than 1 s; only the first three points are indicative for the propene oxidation over this catalyst.

With this catalyst, all the products should be formed at contact times close to zero, which illustrates the fast progress of the reaction. Acrylic acid is the main product, followed by acrolein, acetic acid, CO_x, and acetone. The nature of the trends for each of them at contact times less than 1 s may give some indication of the sequence of their formation, as in the previous cases.

Again, acetic acid formation does not show any relationship with CO_x formation at the contact times studied. A closer look at how the relationship between AcA and CO_x varies for the three catalysts studied shows that with an increase in catalyst activity, CO_x formation requires much higher contact times to match the selectivity to acetic acid. This direct relationship between catalyst property (performance) and acetic acid/CO_x formation supports the proposed explanation of different kinetics for the formation of each of these products.

In short, it is observed that in moving from an air-calcined sample, to a nitrogen-calcined sample activated in O_2/He, to a nitrogen-calcined sample activated in He, catalyst performance improves in both activity and selectivity to acrylic acid.

Combining the results for propene oxidation over the three different catalysts, it is possible to propose a reaction scheme (Scheme 1). There the primary products are acrolein (major) and acetone for all catalysts, which undergo further oxidation to acrylic and acetic acids. The latter can be further transformed to CO_x. The acrylic acid route is the major route with catalysts calcined in nitrogen, whereas for the catalyst calcined in air, the acetic acid pathway is slightly favoured. Additionally, propionic acid is formed in small amounts, but the necessary intermediates are not detected. The selectivity to propionic acid does not decline with contact time, which suggests that it is a more stable product than acrylic and acetic acids under these conditions and probably does not oxidise further to yield CO_x.

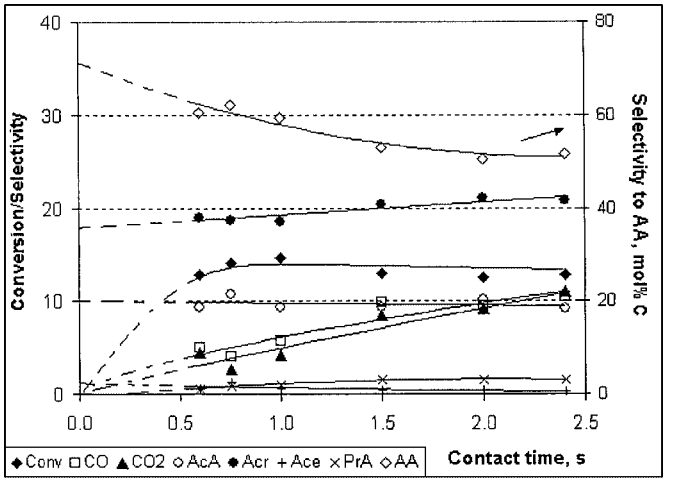

FIG. 6. Conversion/selectivity (mol% C) vs contact time for propene oxidation with catalyst calcined at 500°C in nitrogen, activated at 500°C in He (abbreviations as in Fig. 4).

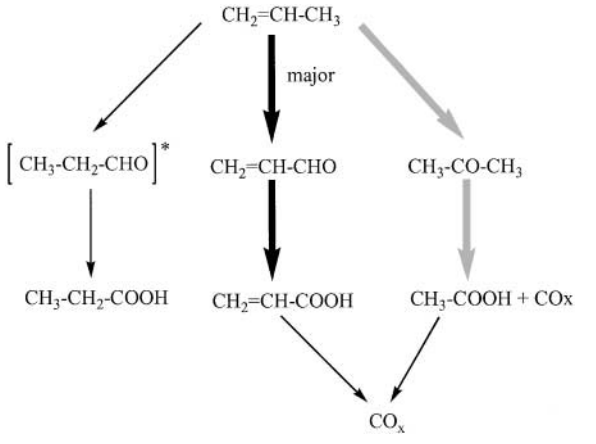

SCHEME 1. Proposed reaction network for propene oxidation over Mo–V–Sb–Nb mixed oxide catalyst. Thick black and grey arrows, preferred pathways for nitrogen- and air-calcined catalysts, respectively; ∗, not detected.

Propane Oxidation

Literature results (1, 13, 22) suggest than propane oxidative dehydrogenation to propene is the sole first step of the reaction. But this appears not to be the case with the catalyst calcined in air (23), as shown in Fig. 7. Three products (propene and acetic and acrylic acids) should be detected at zero contact time, but the shape of their trends suggests that propene as well as acetic acid are the primary products. The curve for propene selectivity decreases more rapidly, which indicates that it is a key intermediate which is quickly consumed in the next steps of the reaction. The acetic acid curve also declines with contact time, but at a much slower rate. The lack of dependence between propene and acetic acid formation (as established with propene oxidation) leads to the conclusion that in this case the latter was formed via a route bypassing propene as intermediate. This is supported by literature data (21), where an alternative route was proposed, with initial formation of isopropanol, which further oxidises to acetone and acetic acid. It was speculated that at high temperatures, isopropanol and acetone are highly reactive and exist only as surface-adsorbed species.

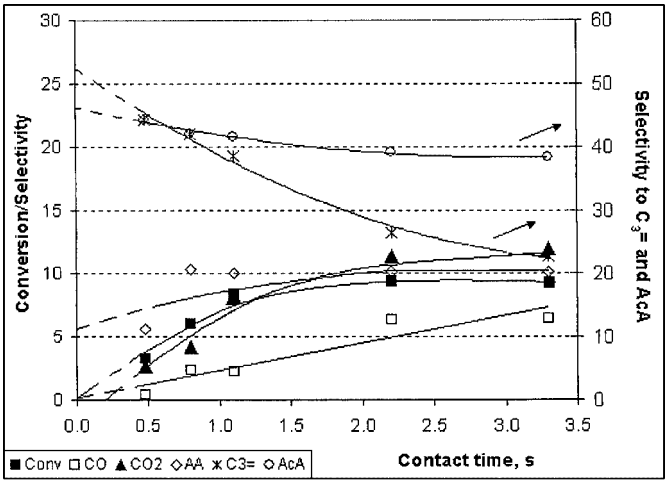

FIG. 7. Conversion/selectivity (mol% C) vs contact time for propane oxidation with catalyst calcined in at 600°C in air, activated at 500°C in O_2/He (abbreviations as in Fig. 4).

Despite the fact that the extrapolated values of the selectivity to acrylic acid give a positive intercept at 0-s contact time, its shape indicates that it is a secondary product, similar to that of propene oxidation over the same catalyst.

The extrapolation of CO_2 and CO selectivities to 0-s contact time shows that they should be formed at very low positive contact times. Their selectivities increase nearly linearly with contact time to about 2.2 s and then become constant. These trends seem to be more similar to an acetic acid curve than to an acrylic acid one.

Propane oxidation experiments performed over the nitrogen-calcined catalysts activated in O_2/He demonstrated again better catalytic performance than the air-calcined samples (Fig. 8). At zero contact time all products are formed.

The level of propene decreases again with contact time, but after 1.2 s it reaches a constant value. With this catalyst, acrolein and acetone are also detected and their curves show the same behaviour as those obtained from propene oxidation.

The trend for acrylic acid starts from 20% selectivity, increases with contact time, passing through a maximum at about 30 mol% C, and then starts decreasing. This shape can be attributed to a product which is formed in the process of the reaction and partially consumed in subsequent steps.

A significant difference in the route of acetic acid formation is observed with this catalyst. In the case of catalyst calcined in air, propane oxidation via an isopropanol intermediate was postulated as the major pathway leading to acetic acid formation. With the nitrogen-calcined catalyst, the selectivity towards acetic acid is lower and the curve increases with contact time, as for a secondary product. In addition, acetone was also detected. Therefore, it can be concluded that over this catalyst, the major route for acetic acid formation goes through propene as a primary intermediate.

The selectivities to CO_x steadily increase with contact time. The shape of their trend does not match with the one of acetic acid, which indicates that these are formed from both acrylic and acetic acids as a result of overoxidation and C–C cleavage. Propionic acid is formed in very small amounts, with selectivities well below 1%.

As for propene oxidation, propane oxidation over the catalyst calcined at 500°C in nitrogen and activated in helium shows a propane conversion higher than that of the previous two catalysts studied, approaching the theoretical maximum of 12.5% for total oxidation (Fig. 9). Again, all the products are detected at zero contact time. Propene decreases linearly with contact time from 54 (extrapolated

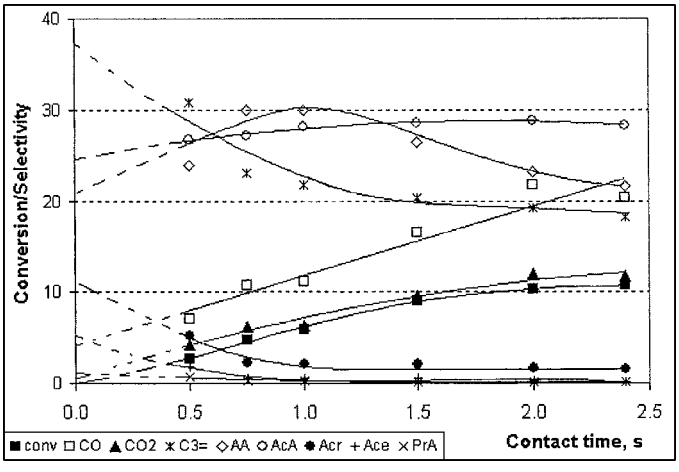

FIG. 8. Conversion/selectivity (mol% C) vs contact time for propane oxidation with catalyst calcined at 500°C in nitrogen, activated at 500°C in O_2/He (abbreviations as in Fig. 4).

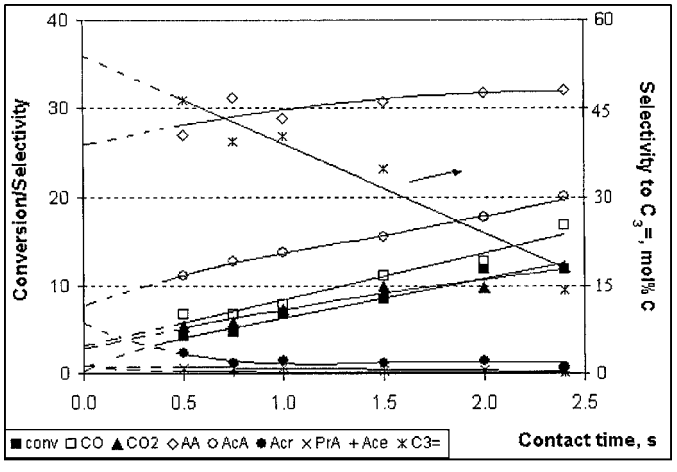

FIG. 9. Conversion/selectivity (mol% C) vs contact time for propane oxidation with catalyst calcined at 500°C in nitrogen, activated at 500°C in He (abbreviations as in Fig. 4).

value) to 14 mol% C. Acetone and acrolein curves also decrease. With this catalyst, acrylic and acetic acids steadily increase with contact time, typical for secondary products. As discussed for propene oxidation over the same catalyst, this reaction goes predominantly to acrylic acid. CO_2 and CO behaviour with contact time are the same as in the previous case and their selectivities increase nearly linearly.

Propionic acid is still formed with selectivities less than 1%, which is too low for detailed investigation. The only conclusion which could be drawn is that it is definitely formed through propene, as its amount does not change even with the introduction of propane rather than propene in the feed.

All this clearly shows that propane oxidation over this sample goes mainly or completely through the formation of propene as a first step of the reaction.

Reaction Network for Propane Oxidation over Mo–V–Sb–Nb Mixed Oxide Catalysts

Propane oxidation over the three catalysts studied show two major features.

- It follows the trends obtained for propene oxidation over the same catalysts.
- It differs significantly from catalyst to catalyst, especially between those calcined under air and under nitrogen.

The origin of acetic acid seems to be the main question that must to be answered in order to determine the reaction pathways. In the case of nitrogen-calcined catalysts, the results show that acetic acid is formed via propene and, therefore, the first step of the reaction is an oxidative dehydrogenation of propane to propene. This statement is supported by the results from propene oxidation reactions, where close behaviour in selectivity vs contact time curves is observed.

In the case of the air-calcined catalyst, a significant difference is observed between the propane and propene oxidation results with respect to acetic acid. For propane oxidation reaction, acetic acid shows the behaviour of a primary product, while during propene oxidation, it is a typical secondary product, which starts to be formed at positive contact time. Therefore, with the air-calcined catalyst, it can be proposed that acetic acid is formed mainly through a reaction pathway which bypasses propene as an intermediate and only a small part of it is formed via propene. There is no evidence from the reaction results of the nature of the intermediates leading to acetic acid, but one possibility, reported in the literature, is the formation of isopropanol. With these data taken into account, a reaction network for the direct oxidation of propane over Mo–V–Sb–Nb mixed oxides catalysts can be proposed as outlined in Scheme 2.

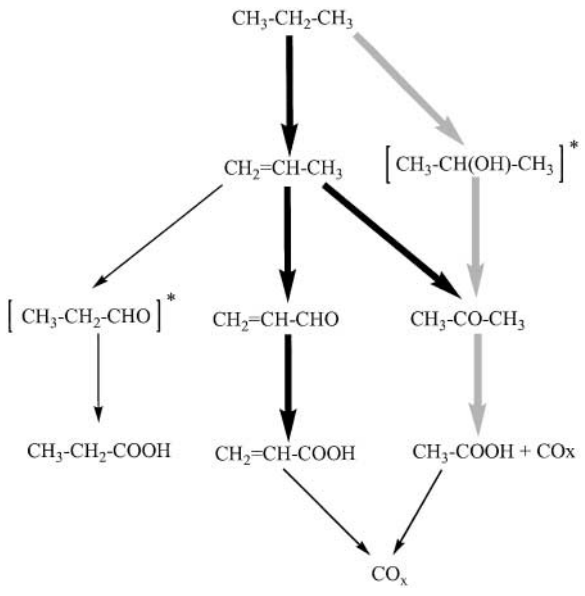

SCHEME 2. Proposed reaction network for propane oxidation over Mo–V–Sb–Nb mixed oxide catalysts. Thick black and grey arrows, preferred pathways for nitrogen- and air-calcined catalysts, respectively; ∗, not detected.

Correlation between the Testing Results and the Physical Properties of the Catalysts in Propane Oxidation Reactions

The differences in the reaction pathways can be attributed to the different physical properties of these catalysts (crystalline phases and redox and acidity properties), crucial for processes where the Mars–van Krevelen mechanism operates. A direct relationship between the physical properties and the catalytic performance of differently calcined samples was established, implying that the best results in terms of propane conversion and selectivity to acrylic acid are obtained with a catalyst calcined at 500°C in nitrogen and activated at 500°C in He. This catalyst possesses a number of mixed oxide phases: $Sb_4^{3+}Mo_{10}^{5+}O_{31}$, $Mo_8^{5.75+}O_{23}$, and $(M_yMo_z^{5+}Mo_{1-y-z}^{6+})_5O_{14}$-type phases, where $M = V$ ($y = 0.09$, $z = 0.31$) and/or Nb ($y = 0.07$, $z = 0.33$), which are clearly constituted by partially reduced metal cations. This was further confirmed by TPR, XPS, and ESR analyses.

The catalyst calcined at 600°C in air and activated at 500°C in O_2/He has MoO_3 as a major phase together with Mo_8O_{23}, $VSbO_4$, and $(M_yMo_z^{5+}Mo_{1-y-z}^{6+})_5O_{14}$-type phases. This catalyst is characterised by a higher total oxidation state compared to that of the previous catalyst and by slightly higher acidity. With the catalyst calcined in air, the acetic acid route was determined as a major reaction pathway; furthermore, it goes via first intermediate, which is different from propene. The enhancement of the C–C cleavage reaction can be attributed to the presence of a MoO_3 phase, which has been shown to be active in terms of oxygen

insertion, but not selective towards acrylic acid. Additionally, the acidic function of this catalyst can also facilitate this type of reaction. It is important to emphasise that the MoO_3 phase is absent in the catalyst calcined in nitrogen and activated in helium and in this case a significant decrease in the formation of acetic acid is observed at the expense of acrylic acid.

With the nitrogen-calcined catalyst activated in inert atmosphere (He), the first intermediate was solely attributed to propene. This can be understood with the partially reduced state of all phases in this catalyst, i.e., lower lattice oxygen concentration for oxygen insertion into the hydrocarbon. The major oxygenated product obtained with this catalyst is the acrylic acid. We belive that the major factor for this behaviour is the presence of the complex mixed oxide phases, in particular $Sb_4Mo_{10}O_{31}$ in synergy with $(M_yMo_z^{5+}Mo_{1-y-z}^{6+})_5O_{14}$-type phases. The latter phase is based on a Mo_5O_{14} oxide structure, in which V and/or Nb atoms are dissolved in the penta- and hexagonal windows of the oxide. It is suggested in the literature that the intergrowth between $Sb_4Mo_{10}O_{31}$ and $(M_yMo_z^{5+}Mo_{1-y-z}^{6+})_5O_{14}$-type phases contributes to the active phase in propane ammoxidation reaction (25, 26). Other literature sources also reiterate the importance of these types of phases in the formation of acrylic acid (10, 15, 19, 26–29). However, there is no definitive evidence that these are the active phases for this type of catalyst.

The catalyst calcined at 500°C in nitrogen and activated at 500°C in an oxidative atmosphere (20% O_2/He) has slightly different crystalline phase distribution than that of the nitrogen-calcined sample activated in He, as the major $Sb_4^{3+}Mo_{10}^{5+}O_{31}$ phase is fully transformed to the more oxidised $Sb_2^{5+}Mo_{10}^{5.2+}O_{31}$ phase. This results in slightly lower propane conversion and selectivity of acrylic acid at the expense of acetic acid selectivity. Thus, in order to direct the reaction towards the desired product (acrylic acid), Sb–Mo–O and $(M_yMo_z^{5+}Mo_{1-y-z}^{6+})_5O_{14}$ phases must be present, and furthermore, they need to be in partially reduced state, as in the $Sb_4^{3+}Mo_{10}^{5+}O_{31}$ phase.

CONCLUSIONS

Based on the results of propane and propene oxidations over the three catalysts, some aspects of the mechanism of the propane oxidation reaction and its relationship with the physical properties of the catalysts become apparent.

- This study confirmed the previous observations that the propane oxidation reaction network is sensitive towards the physical state of the catalyst, which is determined by the calcination and activation procedures.
- The catalyst performance closely follows presence of specific crystalline phases. The activity and selectivity to acrylic acid improve in order from air-calcined samples, to nitrogen-calcined samples activated in O_2/He, to nitrogen-calcined samples activated in He. This is assigned to the diminishing presence of the MoO_3 phase and to the increasing formation of the $Sb_4Mo_{10}O_{31}$ and/or $(M_yMo_z^{5+}Mo_{1-y-z}^{6+})_5O_{14}$-type phases, where $M = V$ ($y = 0.09$, $z = 0.31$) and/or Nb ($y = 0.07$, $z = 0.33$).
- The propene oxidation study identified acrolein as a major primary product over the three catalysts. Acrylic acid is the main secondary product with nitrogen-calcined catalysts (i.e., major reaction pathway), whereas with air-calcined samples, the acetic acid route prevails over the acrylic acid one. These trends are even more pronounced when propane oxidation is conducted. The main reason for the observed differences lies in the presence of different crystalline phases, as established above, and in the partial reduced state of all metal cations in the crystalline phases present as well as in the lower acidity of the nitrogen-calcined samples, which leads to preferential formation of propene and acrylic acid.
- Propane oxidation reactions suggest that acetic acid is formed from the propene primary product via acetone, as mentioned above, or via an isopropanol intermediate to acetone and then acetic acid. The isopropanol intermediate is not detected during the experiments. The former route is preferred with nitrogen-calcined samples, while the latter is the main route with air-calcined samples.

ACKNOWLEDGMENTS

The authors thank Dr. D. Murphy from Cardiff University for the ESR analyses and Mrs. M. Brun from Institut de Recherches sur la Catalyse, CNRS, Lyon for the XPS analyses.

REFERENCES

1. Ai, M., *J. Catal.* **101**, 389 (1986).
2. Ai, M., *Catal. Today* **13**, 679 (1992).
3. Han, Y., Wang, H., Cheng, H., and Deng, J., *J. Chem. Soc. Chem. Commun.* 521 (1999).
4. Volta, J. C., *Catal. Today* **32**, 29 (1996).
5. Cavani, F., and Trifiro, F., *Catalysis* **11**, 246 (1994).
6. Mizuno, N., Tateishi, M., and Iwamoto, M., *Appl. Catal. A* **128**, L165 (1995).
7. Ueda, W., and Suzuki, Y., *Chem. Soc. Jpn. Chem. Lett.* 541 (1995).
8. Li, W., and Ueda, W., *Stud. Surf. Sci. Catal.* **110**, 433 (1997).
9. Li, W., Oshihara, K., and Ueda, W., *Appl. Catal. A* **182**, 357 (1999).
10. Ueda, W., and Oshihara, K., *Appl. Catal. A* **200**, 135 (2000).
11. Baerns, M., Buyevskaya, O. V., Kubik, M., Maiti, G., Ovsitser, O., and Seel, O., *Catal. Today* **33**, 85 (1997).
12. Barrault, J., Batiot, C., Magaud, L., and Ganne, M., *Stud. Surf. Sci. Catal.* **110**, 375 (1997).
13. Kaddouri, A. C., Mazzocchia, C., and Tempesti, E., *Appl. Catal. A* **180**, 271 (1999).
14. Kim, Y.-C., Ueda, W., and Moro-oka, Y., *Appl. Catal.* **70**, 175 (1991).
15. Lin, M., *Appl. Catal. A* **207**, 1 (2001).
16. Mitsubishi Chemicals, U.S. Patent 5,472,925 (1995).
17. Ushikubo, T., Oshima, K., Kayou, A., Vaarkamp, M., and Hatano, M., *J. Catal.* **112**, 394 (1997).
18. Mitsubishi Chemicals, Jpn. Patent 10-36311 (1998).

19. Watanabe, H., and Koyasu, Y., *Appl. Catal. A* **194–195**, 479 (2000).
20. Lin, M., and Linsen, M. W., Eur. Patent 0962253-A3 (1999), assigned to Rohm-Haas.
21. Lin, M., Desai, T. B., Kaiser, F. W., and Klugherz, P. D., *Catal. Today* **61**, 223 (2000).
22. Luo, L., Labinger, J. A., and Davis, M. E., *J. Catal.* **200**, 222 (2001).
23. Novakova, E. K., Védrine, J. C., and Derouane, E. G., *J. Catal.* **211**, 226 (2002).
24. Novakova, E. K., Ph.D. thesis. Liverpool University, 2002.
25. Aouine, M., Dubois, J. L., and Millet, J. M. M., *Chem. Commun.* 1180 (2001).
26. Dieterle, M., Mestl, G., Jäger, J., Uchida, Y., Hibst, H., and Schlögl, R., *J. Mol. Catal. A* **174**, 169 (2001).
27. Thorsteinson, E., Wilson, T., Young, F., and Kasai, P., *J. Catal.* **52**, 116 (1978).
28. Oshihara, K., Hisano, T., and Ueda, W., *Topics Catal.* **15**, 153 (2001).
29. Ruth, K., Burch, R., and Kieffer, R., *J. Catal.* **175**, 27 (1998).